Scanning probe-induced thermoelectrics in a quantum point contact: Supplementary Material

Geneviève Fleury,[1] Cosimo Gorini,[1] and Rafael Sánchez[2]
[1)] *Université Paris-Saclay, CEA, CNRS, SPEC, 91191, Gif-sur-Yvette, France*
[2)] *Departamento de Física Teórica de la Materia Condensada, and Condensed Matter Physics Center (IFIMAC), Universidad Autonoma de Madrid, 28049 Madrid, Spain*

(Dated: 12 July 2021)

As in the main text, we fix $L_x = 100a_0$, $L_y = 5a_0$, $a = 0.5a_0$, and $t = t_0(a_0/a)^2$, $a_0 \equiv 1$ and $t_0 \equiv 1$ being our space and energy units.

I. FINITE-SIZE EFFECTS

The low-temperature transport coefficients $\bar{S}_{LT}$, $\bar{S}_{LL}$, and $\bar{G}_{LL}$ are strongly dependent on the ribbon width W. As noticed in the main text, the 2DEG limit ($W \to \infty$) is guaranteed at finite W as long as the tip is moved in a small region around the QPC center (the smaller W, the smaller the region). Outside this region, additional scattering against the ribbon boundaries become relevant. We show in Fig.S1 how the interference patterns of $\bar{S}_{LT}$ vary when W is increased, keeping fixed the lattice spacing a. For small $\mu = 0.2$ (*i.e.* when the QPC is tuned to its first transmission step, top panel in Fig.S1), finite-width effects along the axis $y_T = 0$ are negligible for $|x_T| \lesssim 80$ and $W \geq 100$, and we check that $\bar{S}_{LT} \to 0$ at large $|x_T|$. At larger $\mu = 0.8$ (*i.e.* when the QPC is tuned to its second transmission plateau, bottom panel in Fig. S1), stronger finite-width effects in W appear at large x_T. They prevent us from providing a rigorous numerical proof of the cancellation of $\bar{S}_{LT}$ away from the QPC, in the 2DEG limit. This would require longer calculations that we did not run.

II. DEPENDENCE OF THE TRANSPORT COEFFICIENTS ON THE TIP-2DEG COUPLING

The amplitude of the tip-induced oscillations of the low-temperature transport coefficients $\bar{S}_{LT}$, $\bar{S}_{LL}$, and $\bar{G}_{LL}$ increases with the tip-2DEG hopping term t_T. We find numerically that $\bar{S}_{LT}/(t_T/t)^2$, $(\bar{S}_{LL} - \bar{S}^0_{LL})/(t_T/t)^2$, and $(\bar{G}_{LL} - \bar{G}^0_{LL})/(t_T/t)^2$ are (almost) independent of t_T in the low coupling limit ($t_T \ll t$). This is illustrated in Fig. S2.

III. TRANSMISSION PLOTS

In the low temperature limit and within linear response regime, the (dimensionless) local and non-local thermopowers $\bar{S}_{LL}$ and $\bar{S}_{LT}$ are controlled by the transmissions τ_{RL}, τ_{LT}, τ_{TR} and their derivatives $\partial_E\tau_{RL}$, $\partial_E\tau_{LT}$, $\partial_E\tau_{TR}$, through Eqs. (8) and (12) of the main paper (with $\tau_{\alpha\beta} = \tau_{\beta\alpha}$ for $\alpha, \beta = L, R$ or T). To understand the behavior of $\bar{S}_{LL}$ and $\bar{S}_{LT}$ with the tip, it is therefore instructive to investigate how the transmissions $\tau_{\alpha\beta}$ and their derivatives $\partial_E\tau_{\alpha\beta}$ vary when the tip is moved above the 2DEG. Our results are summarized in Figs. S3 and S4. In those figures, the tip is moved along the x axis at fixed $y_T = 0$ or $y_T = 3$.

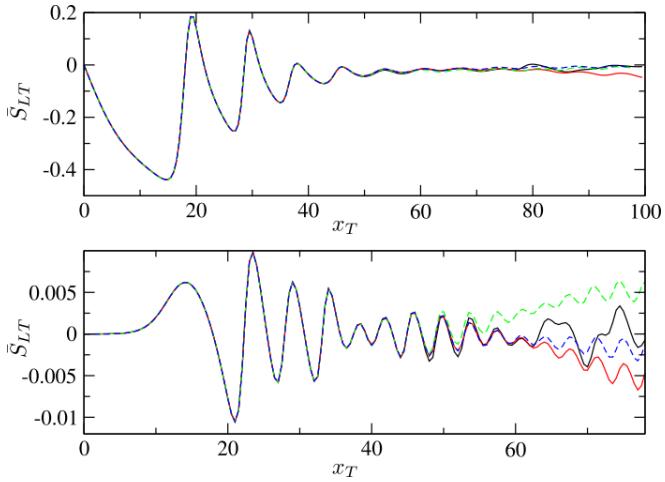

FIG. S1. Non local thermopower $\bar{S}_{LT}$ in the low temperature limit as a function of the tip position x_T, for various values of the ribbon width W ($W = 100$ (black line), 500 (red line), 1000 (green dashed line), and 2000 (blue dashed line)). Data are shown for $\mu = 0.2$ (top panel) and $\mu = 0.8$ (bottom panel). In both panels, $y_T = 0$ and $t_T = 0.1t$.

In Fig. S3, we see that for $\mu \lesssim 0.2$ *i.e* when $\tau_0(\mu) = 0$ (see Fig. 1 of the main paper), the left-to-right transmission of the three-terminal device vanishes ($\tau_{RL} = \tau_0 = 0$) since the QPC is closed. However, if the tip is placed between the QPC and the left lead, electrons coming from the tip can flow towards the left lead, after a sequence of bounces against the QPC barrier. This explains why interference fringes are visible for $x_T < 0$ at small $\mu \lesssim 0.2$ in the colormaps of $\tau_{LT}(x_T, \mu)$ shown in Fig. S3 (third column). For symmetry reasons, the same behavior is observed for $\tau_{TR}(x_T) = \tau_{LT}(-x_T)$ (last column of Fig. S3). When μ is increased so as one electronic mode can be transmitted through the QPC ($0 < \tau_0(\mu) \leq 1$), τ_{RL} increases. The latter is almost unaffected by the presence of the tip on the first QPC plateau while deviations of τ_{RL} from its value τ_0 without tip are relevant around the first QPC step. In all cases, $\tau_{RL}(x_T) = \tau_{RL}(-x_T)$. On the contrary, the colormaps of τ_{LT} (and τ_{TR} as well) are strongly asymmetric with respect to the axis $x_T = 0$. When μ is increased further so as $1 < \tau_0(\mu) \leq 2$, the second QPC channel comes into play. Due to its V-shaped spatial structure, it has no interplay with the tip if the latter is moved along the axis $y_T = 0$ (top panels

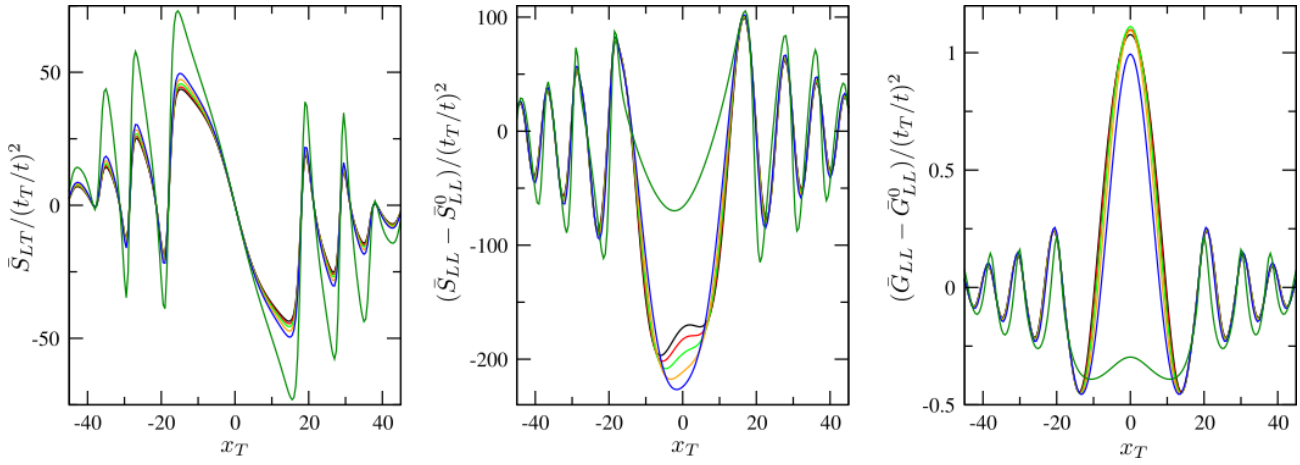

FIG. S2. Tip-induced oscillations of the low-temperature transport coefficients ($\bar{S}_{LT}$ (left), $\bar{S}_{LL}$ (middle), and $\bar{G}_{LL}$ (right)), as a function of the tip position x_T, for different values of the tip-2DEG hopping term t_T ($t_T = 0.01t$ (black line), $0.2t$ (red line), $0.3t$ (green line), $0.4t$ (orange line), $0.5t$ (blue line), and t (dark green line)). After shifting and scaling the data for $\bar{S}_{LT}$, $\bar{S}_{LL}$, and $\bar{G}_{LL}$ along the $y-$axis, the curves of $\bar{S}_{LT}/(t_T/t)^2$, $(\bar{S}_{LL}-\bar{S}^0_{LL})/(t_T/t)^2$, and $(\bar{G}_{LL}-\bar{G}^0_{LL})/(t_T/t)^2$ are nearly superimposed for small $t_T \ll t$. In all panels, $y_T = 0$, $W = 500$ and $\mu = 0.2$.

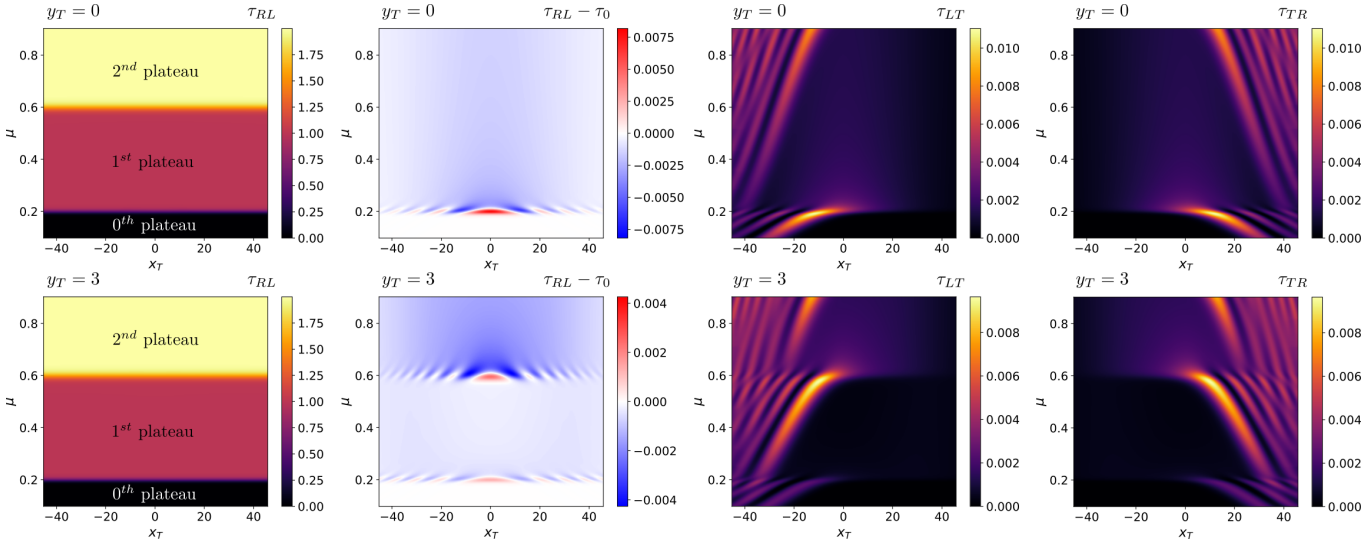

FIG. S3. Transmission maps as a function of μ and x_T for $y_T = 0$ (top line) and $y_T = 3$ (bottom line). From left to right, colormaps are shown for τ_{RL}, $\tau_{RL}-\tau_0$, τ_{LT}, and τ_{TR} evaluated at the energy μ. The three regions where $\tau_0(\mu) = 0$, 1 and 2 (corresponding respectively to the zero-th, first, and second QPC plateau) are clearly visible in the leftmost panels for τ_{RL} since the deviation of τ_{RL} from its value without tip τ_0 is small compared to 2 everywhere. In all panels, $W = 100$ and $t_T = 0.1t$.

in Fig. S3). However, signatures of the opening of the second QPC channel are clearly visible in the different transmission maps along $y_T = 3$ (bottom panels in Fig. S3).

In Fig. S4 (first three lines), we show horizontal cuts of the colormaps displayed in Fig. S3 for four values of μ (0.2, 0.4, 0.595, and 0.8) considered in Figs. 2 and 3 of the main paper and for which the QPC is tuned respectively to its first step, first plateau, second step, and second plateau of conductance. Data are shown for the transmissions τ_{RL}, τ_{LT}, τ_{TR} (red lines) and their derivatives $\partial_E\tau_{RL}$, $\partial_E\tau_{LT}$, $\partial_E\tau_{TR}$ (blue dashed lines). In addition, we also show data for the local thermopower $\bar{S}_{LL}$, obtained using Eq. (12) of the main paper (purple lines in the bottom panels of Fig. S4). On the QPC steps (first and third columns in Fig. S4), $\tau_{LT}, \tau_{TR} \ll \tau_{RL}$ and $\partial_E\tau_{LT}, \partial_E\tau_{TR} \ll \partial_E\tau_{RL}$, so that the local thermopower $\bar{S}_{LL}$ is well approximated by the formula (orange dashed lines in the first and third bottom panels)

$$\bar{S}_{LL} \approx \frac{\partial_E \tau_{RL}}{\tau_{RL}} \quad \text{on the QPC steps} \tag{S1}$$

that neglects the small asymmetry $\bar{S}_{LL}(x_T) \neq \bar{S}_{LL}(-x_T)$. On the QPC plateaus (second and fourth columns in Fig. S4), $\tau_{RL} \approx \tau_0$ while $\partial_E\tau_{RL} \ll \partial_E\tau_{LT}, \partial_E\tau_{TR}$, and so $\bar{S}_{LL}$ is very well approximated by the formula (orange dashed lines in the sec-

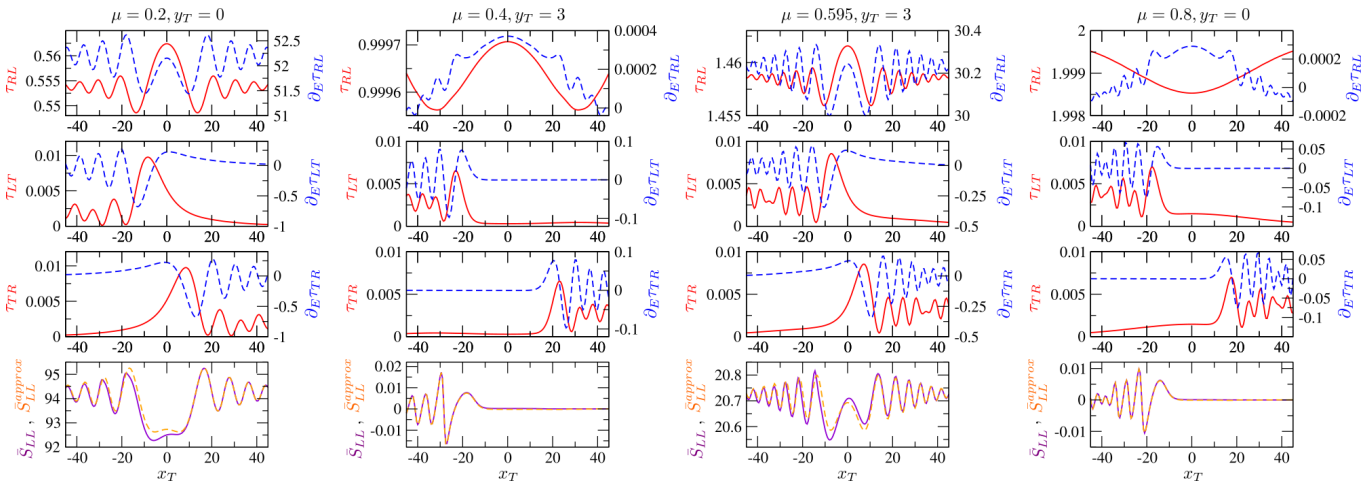

FIG. S4. (First line) τ_{RL} (red full line) and $\partial_E \tau_{RL}$ (blue dashed line) as a function of x_T, along $y_T = 0$ at $\mu = 0.2$ (first column) and $\mu = 0.8$ (fourth column), and along $y_T = 3$ at $\mu = 0.4$ (second column) and $\mu = 0.595$ (third column). (Second line) Same for τ_{LT} (red full line) and $\partial_E \tau_{LT}$ (blue dashed line). (Third line) Same for τ_{TR} (red full line) and $\partial_E \tau_{TR}$ (blue dashed line). Note that $\tau_{TR}(x_T) = \tau_{LT}(-x_T)$. (Last line) Same for the local thermopower $\bar{S}_{LL}$ (purple full line) and the approximate value $\bar{S}_{LL}^{approx}$ (orange dashed line) defined as $\bar{S}_{LL}^{approx} = \partial_E \tau_{RL}/\tau_{RL}$ for $\mu = 0.2$ and $\mu = 0.595$ (*i.e.* on the QPC steps) and as $\bar{S}_{LL}^{approx} = \tau_{TR}\partial_E \tau_{LT}/[\tau_0(\tau_{LT} + \tau_{TR})]$ for $\mu = 0.4$ and $\mu = 0.8$ (*i.e.* on the QPC plateaus). In all panels, $W = 100$ and $t_T = 0.1t$.

ond and fourth bottom panels)

$$\bar{S}_{LL} \approx \frac{\tau_{TR}\partial_E \tau_{LT}}{\tau_0(\tau_{LT} + \tau_{TR})} \quad \text{on the QPC plateaus.} \tag{S2}$$

As a result, $\bar{S}_{LL}$ is finite only when the tip is on the left side of the QPC (*i.e.* the one attached to the hot reservoir) because $\partial_E \tau_{LT} \approx 0$ for $x_T > 0$ while it is finite for $x_T < 0$, and τ_{TR} is also (small but) finite for $x_T < 0$. This explains the origin of the asymmetry in the interference patterns of $\bar{S}_{LL}$ (giving rise to the rectification effect discussed in the main paper) and why this asymmetry is more visible on the QPC plateaus than on the QPC steps.

IV. BEYOND THE COHERENT REGIME

The results described above assume coherent quantum transport through the device, except in the vicinity of the tip playing the role of a scanning voltage probe. We will now investigate (in a phenomenological way) the effects of incoherent scattering on a large scale around the QPC. For that purpose, we introduce in our system fictitious probes mimicking inelastic (electron-electron) scattering. In a region of width W_p and length L_p around the QPC center, we attach to each site S_p in the 2DEG a semi-infinite chain (with lattice parameter a) directed along the axis $z < 0$ and described by the Hamiltonian

$$H_p = -t \sum_{\langle i,j \rangle} c_i^\dagger c_j + \mu \sum_i c_i^\dagger c_i \,. \tag{S3}$$

We denote by t_p the (spatially uniform) hopping term between the site S_p and its nearest neighbor in the probe p. At the energy μ around which transport is investigated, the self-energy of a probe is purely imaginary and reads $\Sigma_p(i,j) = -i(t_p^2/t)\delta_{ij}$. Each probe p is also attached to an electronic reservoir characterized by its temperature θ_p and electrochemical potential μ_p. Their values adjust in such a way that the net average charge and heat currents flowing through the probe vanish (*i.e.* $I_p^e = 0$, $I_p^h = 0$). Contrary to the tip which acts as a voltage probe, those probes do not exchange heat with the 2DEG. Such probes have been used in the literature to model local thermometers.[1–4] Here, we use them to investigate the role of inelastic processes upon the thermoelectric response of our device, in the spirit of Refs. 5–7.

We proceed as follows. We compute the set of $\tau_{\alpha\beta}(\mu)$ and $\partial_E \tau_{\alpha\beta}(E = \mu)$ between the $3 + M$ reservoirs, M being the number of fictitious probes. We deduce (with Eq. (6) of the main paper) the total Onsager matrix (of dimension $[2(M+2)]^2$) in the low temperature limit. Then we write down Eq. (5) of the main paper for the particle and heat currents in the M probes (by noticing that the index β in Eq. (5) now runs over L, T, and the M probes) and we impose the probe condition *i.e.* $I_p^e = 0$, $I_p^h = 0$ to deduce the values of $\Delta\mu_p = \mu_p - \mu$ and $\Delta\theta_p = \theta_p - \theta$ ($p = 1, ..., M$) as a function of $\Delta\mu_L$, $\Delta\mu_T$, $\Delta\theta_L$, and $\Delta\theta_T$. In practice, this requires to solve four systems of $2M$ linear equations. We insert those values into Eq. (5), now written for $\alpha = L$ and T, and define thereby an effective 4×4 Onsager matrix $\tilde{\mathbf{L}}$ that relates through Eq. (5) the particle and heat currents $(I_L^e, I_L^h, I_T^e, I_T^h)$ to the biases $(\Delta\mu_L, \Delta\theta_L, \Delta\mu_T, \Delta\theta_T)$. In the end, we can reproduce the study done in Sections III and IV of the main paper in the presence of incoherent scattering processes by replacing therein the coherent Onsager matrix $\mathbf{L}$ with $\tilde{\mathbf{L}}$. The resulting $\bar{S}_{LT}$, $\bar{S}_{LL}$, and $\bar{G}_{LL}$ are independent of θ in the low temperature limit.

Our results are summarized in Fig. S5. In Fig. S5(a), we show that the conductance $\bar{G}_{LL}^0$ and the thermopower $\bar{S}_{LL}^0$ of the QPC without tip respectively decreases (till vanishing) and

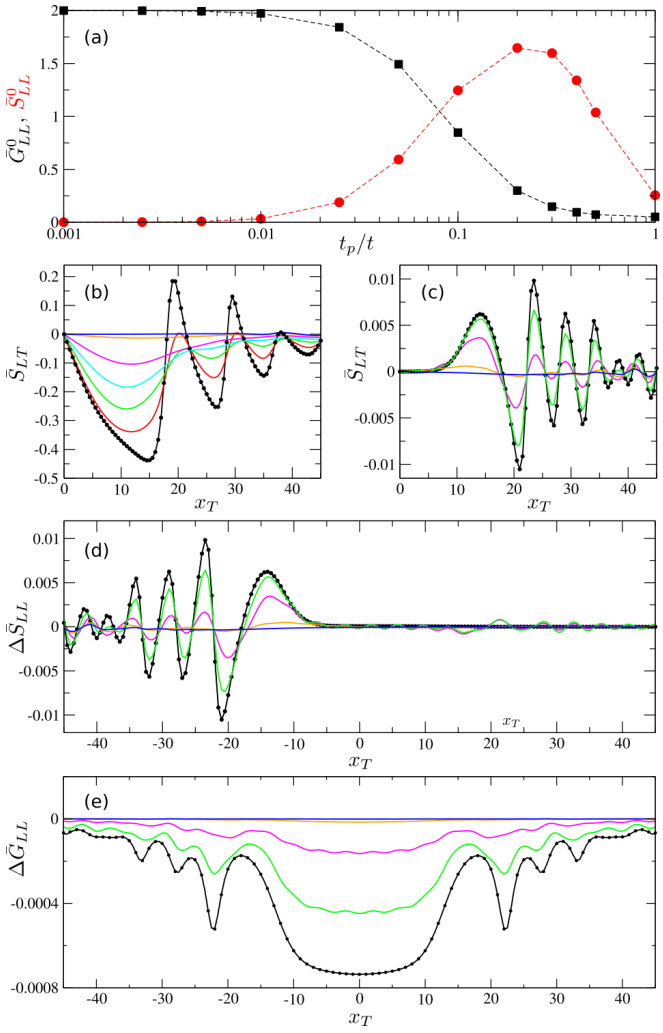

FIG. S5. Effect of fictitious probes on the thermoelectric response. (a) $\bar{G}^0_{LL}$ (black squares) and $\bar{S}^0_{LL}$ (red circles) without tip, as a function of t_p/t, for $\mu = 0.8$. Dashed lines are guides to the eye. (b) $\bar{S}_{LT}(x_T, y_T = 0)$ in the low temperature limit for $\mu = 0.2$ and various values of t_p ($t_p = 0.001t$ (black line), $0.03t$ (red line), $0.05t$ (green line), $0.07t$ (cyan line), $0.1t$ (pink line), $0.2t$ (orange line), and $0.3t$ (blue line)). (c) Same as (b) for $\mu = 0.8$. (d) Same as (c) for $\Delta\bar{S}_{LL} \equiv \bar{S}_{LL} - \bar{S}^0_{LL}$. (e) Same as (d) for $\Delta\bar{G}_{LL} \equiv \bar{G}_{LL} - \bar{G}^0_{LL}$. In panels (b) to (e), data without fictitious probes (corresponding to Figs.2(a), 2(d), 3(d) and 3(h) of the main paper) are shown with black dots. Parameters: $W = 100$, $W_p = 100$, $L_p = 60$, and $t_T = 0.1t$ (except in (a) where $t_T = 0$).

increases (before decreasing and vanishing) with the hopping term t_p. Thus, the fictitious probes become invasive as soon as $t_p \gtrsim 0.1t$: In addition to incoherent scattering processes, they induce backscattering.[8] In Figs. S5(b)-(e), we add the tip and explore how the interference patterns of $\bar{S}_{LT}$, $\bar{S}_{LL}$, and $\bar{G}_{LL}$ are modified in the presence of the fictitious probes. We check first that we recover the coherent limit discussed in the main paper when $t_p \to 0$ (as evidenced by the superposition of dots on black lines in Figs. S5(b)-(e)). As long as the fictitious probes are non invasive (*i.e.* in the weak coupling limit $t_p \lesssim 0.01t$), $\bar{S}_{LT}$, $\bar{S}_{LL}$, and $\bar{G}_{LL}$ are unaffected by the probes. For larger t_p, the tip-induced oscillations of $\bar{S}_{LT}$, $\bar{S}_{LL}$ and $\bar{G}_{LL}$ – around 0, $\bar{S}^0_{LL}$ and $\bar{G}^0_{LL}$ respectively – die out gradually. The present investigation does not allow us however to disentangle the roles of (invasive) backscattering and (noninvasive) incoherent scattering processes. To assess specifically the effect of quantum coherence on the tip-induced thermoelectric effects discussed in the main paper, other models might be considered.[8–11] This is left for future works.

REFERENCES

[1] J. P. Bergfield, S. M. Story, R. C. Stafford, and C. A. Stafford, "Probing Maxwell's demon with a nanoscale thermometer," ACS Nano **7**, 4429 (2013).

[2] J. Meair, J. P. Bergfield, C. A. Stafford, and P. Jacquod, "Local temperature of out-of-equilibrium quantum electron systems," Phys. Rev. B **90**, 035407 (2014).

[3] A. Shastry and C. A. Stafford, "Cold spots in quantum systems far from equilibrium: Local entropies and temperatures near absolute zero," Phys. Rev. B **92**, 245417 (2015).

[4] L. Ye, X. Zheng, Y. Yan, and M. Di Ventra, "Thermodynamic meaning of local temperature of nonequilibrium open quantum systems," Phys. Rev. B **94**, 245105 (2016).

[5] D. Sánchez and L. Serra, "Thermoelectric transport of mesoscopic conductors coupled to voltage and thermal probes," Phys. Rev. B **84**, 201307 (2011).

[6] K. Saito, G. Benenti, G. Casati, and T. Prosen, "Thermopower with broken time-reversal symmetry," Phys. Rev. B **84**, 201306 (2011).

[7] K. Brandner, K. Saito, and U. Seifert, "Strong bounds on Onsager coefficients and efficiency for three-terminal thermoelectric transport in a magnetic field," Phys. Rev. Lett. **110**, 070603 (2013).

[8] R. Golizadeh-Mojarad and S. Datta, "Nonequilibrium green's function based models for dephasing in quantum transport," Phys. Rev. B **75**, 081301 (2007).

[9] C.-L. Chen, C.-R. Chang, and B. K. Nikolić, "Quantum coherence and its dephasing in the giant spin hall effect and nonlocal voltage generated by magnetotransport through multiterminal graphene bars," Phys. Rev. B **85**, 155414 (2012).

[10] H. Förster, S. Pilgram, and M. Büttiker, "Decoherence and full counting statistics in a mach-zehnder interferometer," Phys. Rev. B **72**, 075301 (2005).

[11] H. Rahman, P. Karasch, D. A. Ryndyk, T. Frauenheim, and U. Kleinekathöfer, "Dephasing in a molecular junction viewed from a time-dependent and a time-independent perspective," The Journal of Physical Chemistry C **123**, 9590 (2019).